

MASTER

COO-2479-14

Comp-780921--1

THE MEASUREMENT OF THE ^{238}U (n,γ) CROSS SECTION WITH AN
FE-FILTERED NEUTRON BEAM *

B.L. Quan and R.C. Block
Gaerttner LINAC Laboratory
Rensselaer Polytechnic Institute, Troy, New York 12181

Sept 25-29, 1978

NOTICE

This report was prepared as an account of work sponsored by the United States Government. Neither the United States nor the United States Department of Energy, nor any of their employees, nor any of their contractors, subcontractors, or their employees, makes any warranty, express or implied, or assumes any legal liability or responsibility for the accuracy, completeness or usefulness of any information, apparatus, product or process disclosed, or represents that its use would not infringe privately owned rights.

ABSTRACT

The neutron capture cross section of ^{238}U has been measured near 24.3, 69.8, 80.3, 131.0, 165.9 and 181.4 keV with the Fe-filtered neutron time-of-flight technique. The measured capture cross sections at these energies are respectively (496 ± 15) , (297 ± 22) , (190 ± 9) , (167 ± 6) , (128 ± 7) , and (118 ± 6) mb. The evaluated ENDF/B-IV capture cross section is in satisfactory agreement with the results of this measurement near 24.3 and 131.0 keV, but discrepancies of about 10 to 20 per cent are observed at the other energies.

I. INTRODUCTION

The accurate determination of the ^{238}U (n,γ) cross section in the keV region has been the object of numerous measurements^{1,2,3} for over a decade, but we still do not know this cross section better than 5 to 10% in the 10 to 200 keV region. Sensitivity studies have shown that for both thermal and particularly fast^{4,5,6} reactors, ^{238}U capture is an extremely important cross section. High resolution measurements by Perez et al.⁷, have revealed the existence of significant structure in the capture cross section in the keV region which was once believed to be smoothly varying with neutron energy. However, the accurate magnitude of this cross section has yet to be determined. The measurement is intrinsically difficult because of the low binding energy (4.8 MeV) of the neutron and also because conventional white-source neutron time-of-flight (TOF) capture measurements are typically plagued by large time-dependent backgrounds. As a result the uncertainty in the capture cross section is relatively large in these measurements.

DISTRIBUTION OF THIS DOCUMENT IS UNLIMITED

DISCLAIMER

This report was prepared as an account of work sponsored by an agency of the United States Government. Neither the United States Government nor any agency Thereof, nor any of their employees, makes any warranty, express or implied, or assumes any legal liability or responsibility for the accuracy, completeness, or usefulness of any information, apparatus, product, or process disclosed, or represents that its use would not infringe privately owned rights. Reference herein to any specific commercial product, process, or service by trade name, trademark, manufacturer, or otherwise does not necessarily constitute or imply its endorsement, recommendation, or favoring by the United States Government or any agency thereof. The views and opinions of authors expressed herein do not necessarily state or reflect those of the United States Government or any agency thereof.

DISCLAIMER

Portions of this document may be illegible in electronic image products. Images are produced from the best available original document.

The use of filtered neutron beams in TOF measurements has the advantage of both reducing the time-dependent background and accurately determining this background, thus reducing considerably the uncertainty in the cross section caused by background. This technique has been used at RPI⁸ and elsewhere^{9,10,11}, to obtain accurate local-average cross sections at energies corresponding to the total cross sectional minima in the filter material.

This present measurement¹², uses an iron filter to determine the ^{238}U (n, γ) cross section at neutron energies near 24, 70, 80, 131, 166 and 181 keV, thus spanning an energy interval of importance to fast reactors.

II. EXPERIMENTAL METHOD

The measurements were carried out at the Gaertner LINAC Laboratory using the neutron TOF technique. The 1.25-m-dia. liquid scintillator detector at the 25.64-m flight path and the $^{10}\text{B}_4\text{C}$ -NaI detector at the 28.28-m flight path were used for the capture and neutron flux measurements respectively. The experimental apparatus are shown in Fig. 1. This apparatus and TOF technique are described in detail in earlier publications.¹³

A 20-cm-thick high-purity Armco iron filter was used to obtain bands of filtered neutrons in the keV energy region. This filter was split into a 7.5-cm-thick section inside the accelerator target room at a \approx 3-m flight path and a 12.5-cm-thick section at a \approx 22-m flight path. This arrangement provided an optimum signal-to-background ratio for the capture measurements.

The Fe-filtered capture and neutron flux measurements were each carried out with a composite filter of 20-cm-thick Fe, 0.08-cm-thick Cd, and 0.32-cm-thick Pb in the neutron beam. The accelerator was operated at a repetition rate of 500 s^{-1} , an electron pulse width of \approx 110ns, and at an electron energy of \approx 70 MeV.

In order to normalize the capture data to saturated capture in the 6.67-eV s-wave resonance in ^{238}U , both capture and neutron flux measurements were carried out in which the Fe filter was cycled in and out of the beam, while the Cd and Pb filters were left in the beam. This cyclic measurement enabled the Fe-plus-Cd-plus-Pb-filtered keV capture (or neutron flux) to be directly compared with the Cd-plus-Pb-filtered 6.67-eV saturated capture (or neutron flux). For these normalization measurements the LINAC operated at 300 s^{-1} repetition rate, $\approx 160\text{-ns}$ electron pulse width, and $\approx 70\text{MeV}$ electron energy.

The capture pulse-height spectra were measured for capture at the 6.67-eV resonance and at the 24.3-keV Fe-filtered energy band. These data were used to obtain the ratio of the capture detector efficiencies at these two energies. An auxiliary Fe-filtered neutron detector measurement was also carried out in which a graphite slab replaced the $^{10}\text{B}_4\text{C}$ slab; the graphite thickness was selected to scatter the same number of neutrons as the $^{10}\text{B}_4\text{C}$ slab, and this measurement determined the iodine capture background resulting from scattered neutrons entering the NaI crystals.

The capture sample used in this measurement was a highly enriched ^{238}U ($< 5\text{ppm } ^{235}\text{U}$) metallic sample, 7.68-cm in diameter, and with a thickness of $(2.322 \pm 0.012) \times 10^{-3}$ a/b. This sample was kindly loaned to us by the Oak Ridge National Laboratory.

III. DATA REDUCTION

The experimental capture yield over a limited neutron energy band is defined as

$$\bar{Y}(a_I) = \frac{\eta_n(a_I)}{\eta_Y(a_I)} \frac{\sum_i (C_i - B_i)}{\sum_i (C_i' - B_i')} \quad (1)$$

where \bar{Y} is the experimental capture yield over the neutron energy band a_I , $\eta_n(a_I)$ and $\eta_Y(a_I)$ are the neutron and capture detector efficiencies respectively, C_i is the number of capture counts in time-of-flight channel i , B_i is the number of background counts in the capture detector, C_i' is the number of neutron detector counts in

channel i , and B_i is the number of neutron detector background counts. The sums are taken over those channels which span the neutron energy interval a_I . The capture counting data C_i in the keV energy region are shown in Fig. 2 for the Fe-filtered capture measurement, and the shaded areas represent six energy bands over which the ^{238}U capture cross section is determined in this measurement.

From Eq. (1) above, one can similarly find the capture yield $\bar{Y}(a_J)$ at energy band a_J . Dividing $\bar{Y}(a_I)$ by $\bar{Y}(a_J)$, we obtain

$$\frac{\bar{Y}(a_I)}{\bar{Y}(a_J)} = \frac{\eta_n(a_I)}{\eta_n(a_J)} \frac{\eta_Y(a_J)}{\eta_Y(a_I)} \frac{\sum (C_i - B_i)}{a_I} \frac{\sum (C_i' - B_i')}{a_J} \quad (2)$$

Thus the ratio of capture yields is determined by the ratios of detector efficiencies and the ratios of net (background-corrected) capture and neutron detector counts.

In order to normalize the keV-energy capture yields to the 6.67-eV resonance capture, the Fe filter was cycled in and out the neutron beam, and data were obtained respectively for the 24.3-keV Fe-filtered energy band and for the 6.67-eV resonance region. Let a_I in Eq.(2) represent the energy band near 24.3 keV and a_J represent the energy band near 6.67 eV where the capture rate is saturated. Thus Eq. (2) becomes

$$\bar{Y}(24.3 \text{ keV}) = \frac{\eta_n(24.3 \text{ keV})}{\eta_n(6.67 \text{ eV})} \frac{\eta_Y(6.67 \text{ eV})}{\eta_Y(24.3 \text{ keV})} \frac{\sum (C_i - B_i)}{24.3 \text{ keV}} \frac{\sum (C_i' - B_i')}{6.67 \text{ eV}} \bar{Y}(6.67 \text{ eV}). \quad (3)$$

The saturated capture yield $\bar{Y}(6.67 \text{ eV})$ was calculated with a single-level Monte Carlo multiple scattering code¹⁴ and the ^{238}U resonance parameters listed in BNL-325, Third Edition.¹⁵ The calculated saturated yield was 0.985, of which only about 3% was the result of multiple scattering. Since only the multiple scattering correction depends upon the resonance parameters, the calculated saturated yield of 0.985 is relatively insensitive to modest changes in the ^{238}U 6.67-eV resonance parameters.

The capture detector background B_i was determined in the keV region from the background on either side of the Fe-filtered energy bands, and at 6.67 eV by the background observed above and below this resonance. The background is composed of a time-independent component, such as cosmic rays, activity in the ^{238}U sample, etc., and a time-dependent component resulting from neutron scattering from collimators, air and the ^{238}U sample and subsequent capture in the detector. This background can be represented in the vicinity of a neutron energy band by

$$B_i = a + bt_i^c \quad (4)$$

where a is the time-independent background measured (in TOF) just before the linac is pulsed, t_i is the neutron TOF corresponding to channel i , and b and c are constants fitted to the backgrounds measured on each side of the energy band. This exponential dependence with neutron TOF of the time-dependent background has been observed in previous capture measurements with this detector.¹³ The neutron detector background B_i was determined in a similar manner, and it was also fitted to Eq. (4) in the vicinity of each neutron energy band.

The ratio of neutron detector efficiencies in Eq. (3), $\eta_n(24.3 \text{ keV})/\eta_n(6.67\text{eV})$, was computed by the method of Hockenbury et al.¹⁶ from the ENDF/B-IV boron and carbon cross sections taking into account neutron and gamma-ray multiple scattering in the $^{10}\text{B}_4\text{C}$ slab. The ratio of capture detector efficiencies in Eq. (3), $\eta_\gamma(6.67$

eV)/ $\eta_Y(24.3 \text{ keV})$, was determined from the capture detector pulse-height spectra taken at these two energies. The spectrum fraction was computed as the fraction of pulses occurring in the 3- to 15-MeV gamma-ray bias region, and the ratio of capture efficiencies was set equal to the ratio of spectrum fractions. This ratio was equal to 1.11 ± 0.03 , which shows that the detection efficiency for capture at 6.67 eV is about 11% larger than that at 24.3 keV. The efficiency decrease at 24.3 keV is attributed to the substantial p-wave capture occurring at this energy, and this additional p-wave capture is apparently softening the gamma-ray spectra sufficiently to lead to the lower detection efficiency.

The capture yield $\bar{Y}(a_I)$ for the other Fe-filtered energy bands is determined from the 24.3-keV yield by applying Eq.(2) and obtaining

$$\bar{Y}(a_I) = \frac{\eta_n(a_I)}{\eta_n(24.3\text{keV})} \frac{\eta_Y(24.3\text{keV})}{\eta_Y(a_I)} \frac{\frac{\sum (C_i - B_i)}{a_I}}{24.3\text{keV}} \frac{\frac{\sum (C'_i - B'_i)}{24.3\text{keV}}}{\frac{\sum (C'_i - B'_i)}{a_I}} \bar{Y}(24.3\text{keV}). \quad (5)$$

The ratio of neutron detector efficiencies, $\eta_n(a_I)/\eta_n(24.3 \text{ keV})$, is computed from the method of Hockenbury et al.¹⁶; in addition corrections are applied for the increase in this ratio caused by neutrons scattering from the $^{10}\text{B}_4\text{C}$ slab and subsequently being captured in the iodine of the NaI and detected. This scattering effect was measured with the equivalent thickness slab of carbon, and it amounted to a 1.4% maximum increase in detection efficiency for the higher-energy Fe-filtered energy bands. The ratio of capture detector efficiencies, $\eta_Y(24.3 \text{ keV})/\eta_Y(a_I)$, is affected by the relative change in the spectrum fractions between 24.3-keV capture and higher-energy capture. The major contribution to this change is the increased kinetic energy the neutron brings into the excitation of the ^{239}U compound nucleus. This change in the spectrum fraction was computed by assuming that the pulse-height spectrum at higher energies has the same shape as that at 24.3 keV

but that it is shifted to higher pulse heights by the energy of the neutron minus 24.3 keV. This correction resulted in a spectrum fraction ratio of 0.98 near 130 keV and to a minimum ratio of 0.968 at 181 keV.

IV. RESULTS AND DISCUSSION

The experimental capture yields \bar{Y} for the six neutron energy bands are listed in Table I. Each energy band spans the energy range from E_L to E_H , and these energies correspond respectively to the right and left TOF edges of the shaded regions in Fig. 2. The flux-weighted average energy \hat{E} is defined by

$$\hat{E} = \frac{\sum_{i_L}^{i_H} \left[\frac{(C_i' - B_i')}{\eta_n(E_i)} \right] E_i}{\sum_{i_L}^{i_H} \left[\frac{(C_i' - B_i')}{\eta_n(E_i)} \right]}, \quad (6)$$

where the term in the bracket is proportional to the neutron flux in TOF channel i , and the summation from i_L to i_H corresponds to the energy span from E_L to E_H . The experimental capture yields are listed in column 5 of Table I, and the per cent standard deviation errors in the yield are listed in column 6. Each of these errors is the quadrature sum of the counting statistical error for each energy band and the normalization error. The counting statistical error is derived from both the capture and neutron detector counts, and this varies from energy band to energy band. The normalization error is a systematic error of 3.0% for this experiment, and it is dominated by the error in the measurement of the ratio of the capture spectrum fraction at 6.67 eV to that at 24.3 keV.

The experimental capture yield \bar{Y} in Table I decreases with increasing neutron energy, as would be expected for an average capture cross section which decreases with increasing neutron energy. The total per cent error in \bar{Y} ranges from 3.1% at

the 24.3-keV band to 7.3% at the 64.5-keV band.

The capture cross section for a neutron energy band, $\hat{\sigma}(\hat{E})$, can be derived from the experimental capture yield \bar{Y} by correcting for resonance-self-protection and multiple scattering in the capture sample. The method of Schmitt¹⁷ was used for these corrections for which the average total and scattering cross sections of ^{238}U from ENDF/B-IV were used in the analysis. These corrections decreased from a maximum of 4.9% at 24.3 keV to 4.2% at 181.4 keV, and thus they are relatively insensitive to modest changes in the ^{238}U total or scattering cross sections.

The deduced band-averaged capture cross sections $\hat{\sigma}$ are shown in Table II, together with results from other measurements^{18,19} using Fe-filtered neutron beams and the evaluated capture cross section from ENDF/B-IV. At the 24.3-keV energy band the agreement between the three experimental results is excellent, and all the results overlap within the stated errors. All of the 24.3-keV Fe-filtered-beam results can be combined into a weighted average resulting in a value of 497 ± 13 mb.

In order to compare the Fe-filtered-beam band-averaged capture cross section $\hat{\sigma}$ with the average capture cross section determined over a wider energy region $\bar{\sigma}$, it is necessary to consider two effects: (i) the effect of fluctuations in the cross section, and (ii) the neutron energy at which the average capture cross section should be compared with the band-averaged cross section. The fluctuations in the capture cross section result from the finite number of resonances included in a given energy band. The uncertainty in a local average cross section is approximately equal to $(2/N)^{1/2}$, where N is the total number of levels included in the averaging interval. For ^{238}U the average s-wave level spacing is 17.7 ± 0.7 eV.¹⁵ If we assume that the capture cross section at 24.3 keV consists of approximately half s-wave capture and half p-wave capture, and that the average p-wave level spacing is three times the average s-wave spacing, then we have approximately 540 levels contributing to the capture cross section in this 2.4-keV-wide energy band cross

section. This results in a statistical uncertainty of $\sim(2/540)^{1/2}$, or 6% in the standard deviation of this local average from the average over a much larger energy range. This 6% uncertainty from nuclear statistical fluctuations is considerably larger than the experimental uncertainty of 3.1% from this measurement or the uncertainty of 2.6% from the weighted average of all three experimental Fe-filtered beam results, and thus this represents a large uncertainty for the 24.3-keV energy band data. For the higher energy bands, however, we have much wider energy band widths and also more levels from p-wave capture, both of which contribute to nuclear statistical fluctuations which are much smaller than the experimental errors. Thus, we can neglect the effect of fluctuations caused by nuclear statistics in all but the 24.3-keV neutron energy band result.

The effect of fluctuations in $\hat{\sigma}(24.3\text{keV})$ can be estimated from the high-resolution capture measurements of Perez et al.⁷ The band-averaged cross section $\bar{\sigma}(24.3\text{keV})$ for this measurement is given by

$$\hat{\sigma}(24.3\text{keV}) = \frac{\int_{23.6\text{keV}}^{26.0\text{keV}} \sigma(E) \phi(E) dE}{\int_{23.6\text{keV}}^{26.0\text{keV}} \phi(E) dE}, \quad (7)$$

where $\sigma(E)$ is the high-resolution capture cross section of reference 7 at neutron energy E , $\phi(E)$ is the Fe-filtered neutron flux measured in this experiment, and the integral is taken over the energy band limits. The average cross section $\bar{\sigma}(24.3\text{keV})$ is given by

$$\bar{\sigma}(24.3\text{keV}) = \frac{1}{\Delta E} \int_{\Delta E} \sigma(E) dE, \quad (8)$$

where the average is determined over the energy interval ΔE . For an energy interval $\Delta E=9\text{keV}$ which is approximately centered about the 24.3-keV energy band, the ratio

$\hat{\sigma}(24.3\text{keV})/\bar{\sigma}(24.3\text{keV})$ is equal to 1.00 ± 0.01 . Since the nuclear statistical fluctuations in an energy interval of ≈ 9 keV is much less than the fluctuations in the 24.3-keV energy band, we conclude that the 24.3-keV band-averaged capture cross section, $\hat{\sigma}(24.3\text{keV})$, is equal to the average capture cross section at 24.3keV, $\bar{\sigma}(24.3\text{keV})$.

For the higher-energy bands, the capture cross section can be considered to vary smoothly across an energy band. Thus, the problem in comparing the average cross section $\bar{\sigma}$ with the band-averaged cross section $\hat{\sigma}$ is at what energy should the comparison be made. Thus, one must determine E' from

$$\bar{\sigma}(E') = \hat{\sigma}(\hat{E}) \quad (9)$$

where E' is the energy of the average capture cross section which satisfies this equation. The capture cross section of ^{238}U in the 25 to 200 keV energy region varies approximately as $(E)^{-0.6}$. When this energy dependence is used in Eqs. (7) and (8) and the integrals are carried out for each energy band and a ΔE centered about each band, it turns out that $\bar{\sigma}(\hat{E}) = \hat{\sigma}(\hat{E})$ to within an accuracy of better than 2%. Therefore, the average capture cross section at \hat{E} can be compared directly to the band-averaged capture cross section.

The ENDF/B-IV cross sections at \hat{E} are listed in column 6 of Table 2, and they can be compared to the experimental band-averaged cross sections $\hat{\sigma}$ in columns 3 to 5. The difference between the results of this measurement and ENDF/B-IV are shown in column 7. The results of this experiment are also plotted in Fig. 3 along with the measured capture cross sections of Lindner et al.²⁰ and the smooth ENDF/B-IV data. A comparison of the results in Table 2 or in Fig. 2 shows that the ENDF data are in good agreement with the results of this experiment at 24.3 keV and 131.0 keV. However, the ENDF data are $(20 \pm 9)\%$ lower at 69.8 keV, whereas the ENDF data are higher by $(12 \pm 3)\%$, $(16 \pm 5)\%$ and $(20 \pm 4)\%$ respectively at 80.3, 165.9 and 181.4 keV. On the other hand, as can be seen in Fig. 3, the RPI results are in good

agreement with the activation-measured capture cross sections of Lindner et al.²⁰ at 121, 154 and 198 keV. The ENDF/B-IV evaluated capture cross section in the 100 to 200 keV energy range is much larger than the experimental values and this discrepancy is far outside the experimental errors.

V. CONCLUSIONS

The uses of an Fe-filtered neutron beam has enabled accurate measurements of the ²³⁸U capture cross section to be made near 24.3, 69.8, 80.3, 131.0, 165.9 and 181.4 keV. This technique has the advantage of simple experimental execution, low background, and the accurate determination of the detector background in the vicinity of the energy being measured. Discrepancies of about 10 to 20 per cent are observed between these results and the ENDF/B-IV evaluated capture cross section at four energies, with satisfactory agreement obtained only at 24.3 and 131.0 keV.

TABLE I

NEUTRON ENERGY BANDS AND EXPERIMENTAL CAPTURE YIELDS

<u>Energy Band</u>	<u>E_L (keV)</u>	<u>E_H (keV)</u>	<u>\hat{E} (keV)</u>	<u>\bar{Y}</u>	<u>$\delta\bar{Y}/\bar{Y}$ (%)</u>
1	23.6	26.0	24.3	0.001207	± 3.1
2	64.5	75.7	69.8	0.000723	± 7.3
3	76.5	84.9	80.3	0.000460	± 4.9
4	106.7	141.7	131.0	0.000405	± 3.8
5	155.3	173.1	165.9	0.000309	± 5.5
6	175.6	190.9	181.4	0.000286	± 5.4

TABLE II
CAPTURE CROSS SECTION

Energy Band	\hat{E} (keV)	$\hat{\sigma}(\hat{E})$ (mb)			$\sigma(\hat{E})$ (mb)	$\frac{\sigma_{\text{RPI}} - \sigma_{\text{ENDF/B-IV}}}{\sigma_{\text{ENDF/B-IV}}}$ (%)
		RPI	KUR ¹⁸	BNL ¹⁹		
1	24.3	496±15	500±35	500±38	488	2±3
2	69.8	297±22			247	20±9
3	80.3	190±9			215	-12±3
4	131.0	167±6			169	- 1±4
5	165.9	128±7			152	-16±5
6	181.4	118±6			147	-20±4

ACKNOWLEDGMENTS

The authors wish to express their courtesy to Oak Ridge National Laboratory for lending them the samples and to USERDA for their support.

The assistance of Mr. Robert Pendt during the experimental phase is especially appreciated, and the authors wish to thank the technical staff of the Gaerttner LINAC Laboratory for making this experiment possible.

REFERENCES

1. M.C. Moxon, "The Neutron Capture Cross Sections of ^{238}U in the Energy Region 0.5 to 100 keV", AERE-R-6074, (1969).
2. W.P. Poenitz, "Nucl. Sci. Eng. 57,300 (1975).
3. G. de Saussure, E.G. Silver, R.B. Perez, R. Ingle, H. Weaver, "Nucl. Sci. Eng. 51, 385 (1973).
4. P. Greebler, B.A. Hutchins, C.L. Cowan, "Implications of Neutron Data Uncertainties to Reactor Design", IAEA-CN26/102; Second International Conference on Nuclear Data for Reactor Conference Proceedings, Helsinki, 15-19 June 1970, Vol. 1, p. 17 (IAEA, Vienna, 1970).
5. D.R. Harris, Ph.D. Thesis RPI (1976).
6. J.M. Ryskamp, Master Thesis, RPI (1976).
7. R.B. Perez, R.R. Spencer, G. de Saussure, "The $^{238}\text{U}(n,\gamma)$ Cross Section above the Resonance Region", BNL-NCS-50451, p. 103 (1975).
8. R.C. Block, N.N. Kaushal and R.W. Hockenbury, "Topical Meeting on New Development in Reactor Physics and Shielding", CONF-720901, Book 2, p. 1107 (1972).
9. R.C. Block, Y. Fujita, K. Kobayashi and T. Osaka, "J. Nucl. Sci. & Tech. 12, 1 (1975).
10. N. Yamamuro, T. Doi, T. Hayase, Y. Fujita and R.C. Block, "Fourth Conf. on Nucl. Cross Sect. Tech.", NBS Spec. Publ. 425, Vol. II, p. 802 (1975).
11. K. Kobayashi, Y. Fujita, T. Osaka and R.C. Block, "Nucl. Sci. Eng. 65, 347 (1978).
12. B.L. Quan, Master's Thesis, RPI, 1976.
13. R.W. Hockenbury, Z.M. Bartolome, J.R. Tatarczuk, W.R. Moyer and R.C. Block, "Phys. Rev. 178, 1746 (1969); Z.M. Bartolome, R.W. Hockenbury, W.R. Moyer, J.R. Tatarczuk and R.C. Block, "Nucl. Sci. and Eng. 37, 137 (1969).
14. J.G. Sullivan, G.F. Warner, R.C. Block and R.W. Hockenbury, "A Monte Carlo Code for Neutron Capture Experiments", RPI 328-155, Rensselaer Polytechnic Institute (1969)
15. S.F. Mughabghab and D.I. Garber, BNL-325, 3rd Edition, Vol. I (1973).
16. R.W. Hockenbury, Z.M. Bartolome, W.R. Moyer and R.C. Block, Linear Accelerator Progress Report for Oct. 1966 to Dec. 1966, Pg. 36, Rensselaer Polytechnic Institute.
17. H.W. Schmitt, "Sample Scattering Corrections in Neutron Beam Experiments", Oakridge National Laboratory (1960).
18. N. Yamamuro, T. Doi, T. Hayase, Y. Fujita, K. Kobayashi and R.C. Block, "Measurements of Neutron Capture Cross Sections Near 24 keV", Nuclear Cross Section and Technology Conference, March 3-7, 1975, Washington, D.C.
19. K. Ramawi and R.E. Chrien, "Measurements of 24.3 keV Activation Cross Sections with the Iron Filter Technique", Proceedings of a Conference, Nuclear Cross Sections and Technology Vol. II, 1975, p. 922, BNL 19787.

20. M. Lindner, R.J. Nagle and J.H. Landrum, Nucl. Sci. Eng. 59, 381 (1976).

Figure Captions

- Fig. 1 The Experimental Floor Plan for the Iron-filtered ^{238}U Capture Measurements.
- Fig. 2 The Time-of-Flight Spectrum of ^{238}U Capture with the Iron Filter in the Neutron Beam. The shaded areas are the six energy bands over which capture cross sections are determined in this experiment.
- Fig. 3 The Neutron Capture Cross Section of ^{238}U . The crosses are the results of this experiment; the statistical error is indicated by the vertical bar, the energy band is defined by the horizontal bar, and the intersection is plotted at the flux-weighted average band energy \hat{E} . The circles are from the activation measurements of Lindner et al.²⁰ The smooth curve is the ENDF/B-IV capture cross section.

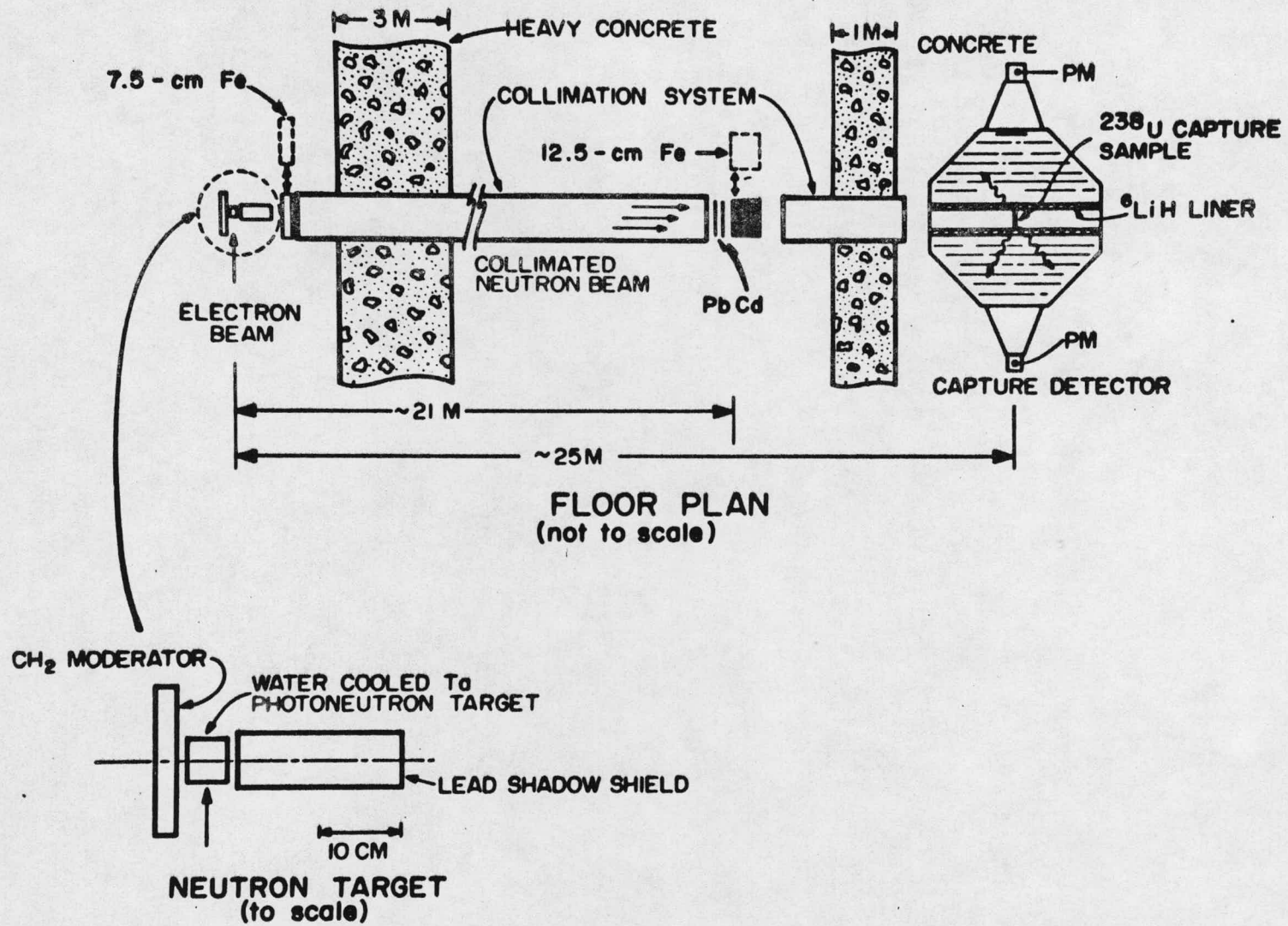


Fig. 1

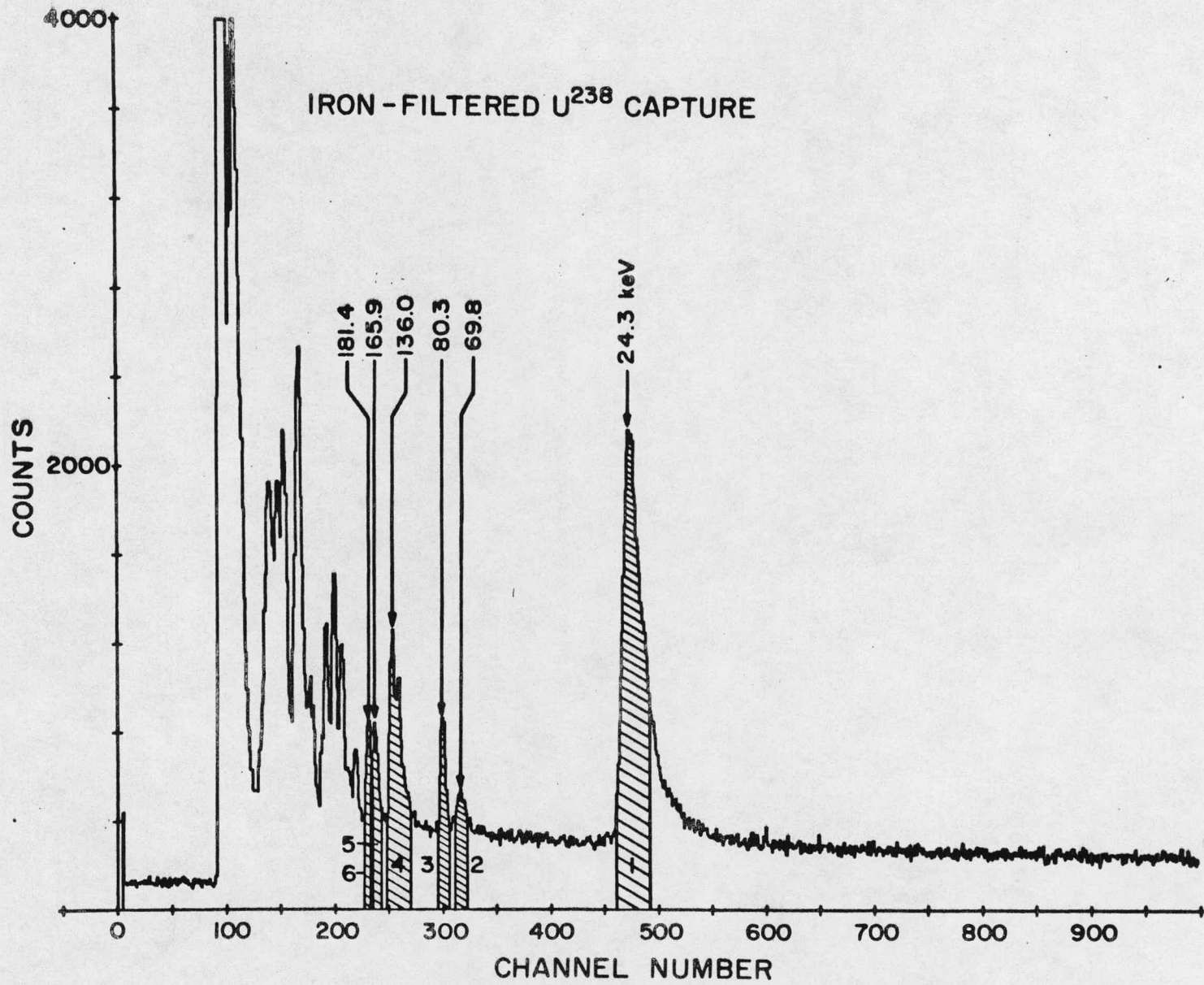


Fig. 2

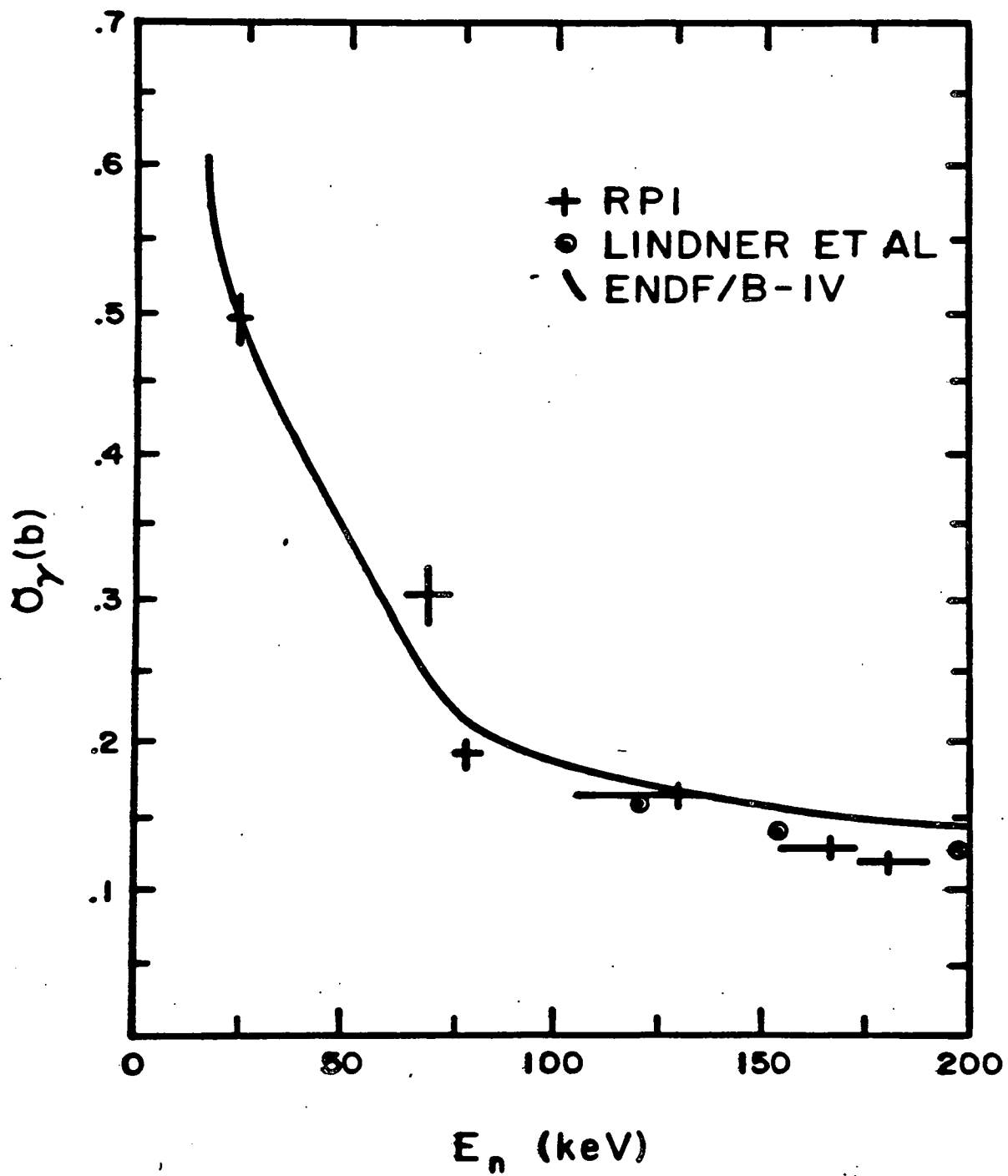


Fig. 3